SLAC-PUB-36
June 1964

LASER BEAM-INDUCED ELECTRON, ION, AND NEUTRAL ATOM EMISSION FROM METAL FOILS*

J. K. Cobb and J. J. Muray

Stanford Linear Accelerator Center
Stanford University, Stanford, California

(Submitted to British Journal of Applied Physics)

*Work supported by U. S. Atomic Energy Commission.

LASER BEAM-INDUCED ELECTRON, ION, AND NEUTRAL ATOM EMISSION FROM METAL FOILS*

J. K. Cobb and J. J. Muray

Stanford Linear Accelerator Center
Stanford University, Stanford, California

ABSTRACT

An experiment was conducted to determine the mechanism involved in electron and positive ion emission from metal foils using a pulsed ruby laser of 0.2 joules output energy. The metals studied, aluminum, silver, gold, beryllium, copper, and stainless steel, were placed in a vacuum chamber at $\approx 10^{-8}$ torr. The surface temperature was calculated from the measured electron current density using the Richardson equation. The total number of electrons emitted was between 7×10^{10} and 0.2×10^{10} electrons per laser burst, while the number of positive ions was between 0.2 and 0.01 of these values. The observed emission can be explained as thermionic emission using the Richardson-Smith equations for electrons and positive ions. The rise and decay of the current pulses are interpreted as a heat conduction process. Effective positive ion work functions for Al, Be, and Cu were found to be 5.3, 5.1, and 7.25 electron volts, respectively. The charged particle current densities are expressed as exponential functions of the input laser beam power.

*Work supported by U.S. Atomic Energy Commission

1. INTRODUCTION

A number of papers concerning the interaction of high intensity light beams with various solid target materials have appeared recently.[1-11] (Linlor 1963; Linlor 1962; Muray 1963; Muray 1964; Honig and Woolston 1963; Lichtman and Ready 1963; Verber and Adelman 1963; Honig 1963; Ready 1963; Giori, MacKenzie and McKinney 1963; Lichtman and Ready 1963.) In these experiments the intensitve light beams were produced by ruby lasers. The energy in the beam varied from a fraction of a joule to a few joules per pulse, and the peak power from kilowatts to several megawatts. The following parameters were investigated in these experiments:

1. The total numbers of the electrons and ions emitted by the metals, semiconductors, and dielectrics
2. The dependence of the output currents on the laser beam power
3. The time correlation of the laser pulse with the electron and ion output pulses
4. The estimated surface temperature, using various theories to explain the electron and ion emission mechanism

2. EXPERIMENTAL PROCEDURE

This experiment was conducted to determine the mechanism involved in electron and positive ion emission from metal foils using a pulsed ruby laser of about 0.2 joules output energy. The metals so studied were aluminum, silver, gold, beryllium, copper, and stainless steel. The foils, each 0.001-inch thick, were placed in a high vacuum chamber with a quartz window so that the laser beam could be focused at the

foil surface. The pressure in the chamber was approximately 10^{-8} mm Hg, as determined by a nude gauge in the chamber near the foils. A schematic diagram of the experimental setup is shown in Fig. 1.

The study consisted of the following investigations:

1. The time correlation of laser pulse, electron output pulse, positive ion pulse, and pressure rise in the vacuum chamber
2. A comparison of electron and positive ion current densities and the total numbers of electrons and positive ions emitted by each metal
3. Estimates of surface temperatures from thermal emission for each metal
4. An explanation of the electron emission pulse shape for each metal using the assumption of a spreading gaussian distribution for the pattern of heat flow in the foils
5. Comparison of the relative numbers of electrons and positive ions emitted at different base pressures
6. Determination of the effective positive ion work function for Al, Be, and Cu

The experiment consisted of simultaneous oscillographic observation of the laser beam pulse by light reflected into a vacuum tube detector, the electron or positive ion pulse on the collector in the chamber, and the pressure change in the chamber caused by the release of free atoms and molecules by the laser beam. The use of a dual beam oscilloscope allowed two time traces to be displayed simultaneously: one time scale for the two traces of laser light pulse and electron and positive ion output, and the other, longer time trace for the

pressure rise readout, which was made through a differential amplifier for easy observation of small pressure changes from the base pressure. The laser beam emitted by a 1/4 × 2-inch ruby crystal at liquid nitrogen temperature, silvered at one end, was focused by an external lens through the window onto the target foils. A one-inch-diameter stainless steel wire ring, located 1/2 inch from the target foil and with the plane of the diameter parallel to the foil, served as the collector. The collector was made positive or negative with respect to the grounded target foil, the charge depending on whether it was desired to collect electrons or positive ions. The collection pulse was the voltage developed across a 1 megohm resistor to ground; it was detected on an oscilloscope with a 1 megohm input resistance.

In the experimental technique, a positive or negative potential was applied to the collector, and the focused laser beam was aimed at the target foil. An oscilloscope photograph was then taken of the collection pulse, the laser pulse as shown by the detector, and the pressure change in the chamber. The trigger for the oscilloscope was the laser pulse itself. The laser and collection pulses were displayed at 50 microseconds per centimeter, while the pressure rise was recorded at 0.2 seconds per centimeter. A typical oscilloscope photograph is shown in Fig. 2.

It was observed that in every case the maximum of the electron output coincided with the end of the laser burst, leading one to the conclusion that the time integral of the photon pulse is the important quantity rather than the magnitude of the laser pulse. This can be interpreted to indicate that the local thermal emission of the foil,

rather than the photoelectric effect, is occurring. The pulse length of the laser pulse varied with the capacitor bank voltage, those with higher voltages being shorter. If the electron output were all thermal emission, one would expect that the maximum electron output would also be delayed approximately the same time as the pulse length; that is, the output electron maximum should occur at the end of the laser pulse in every case. Such is seen to be the case in Fig. 3, where the pulse length of the laser can be compared with the delay from the start of the laser pulse to the maximum electron output and also with the delay of the observed maximum positive ion output.

It was concluded that the maximum surface temperature T of the metal foil in the focused beam spot was that calculable from the Richardson equation,

$$j = AT^2 \, e^{-\frac{\Phi e}{kT}}$$

where j = current density, Φ = electron work function, k = Boltzmann constant, and $A = 120$ amp/cm^2. The physical constants used are listed in Appendix A. The beam spot size of the focused beam which was ascertained by burning paint off a sheet of paper, was found to be 1.7 mm^2. Using the Richardson equation, the maximum temperatures of the surfaces of the foils were determined as listed in Table I.

Two other considerations indicated that the emission was primarily thermal rather than photoelectric. First, the photoelectric work functions of the metals studied were all considerably higher than the quantum energy of the laser, which for 6943°A is 1.78 electron volts. Any photoelectric emission would be simultaneous with the laser pulse,

but in this case a definite time delay was observed between the laser pulse and the electron or positive ion emission.

Secondly, an attempt was made to explain electron output decay from the maximum value using the assumption of a gaussian temperature distribution of full width at one-half maximum of laser beam size. It was assumed that the gaussian would decay to larger widths with time as indicated by the calculated thermal diffusivity for the metals, and from that, changes in the current output with time could be calculated. The results of this calculation are shown in Fig. 4, and the striking agreement with experiment in the cases of copper, gold, silver, aluminum, and beryllium can be seen. Appendix B is the discussion of the gaussian treatment.

Accompanying the first few laser bursts after a metal foil had been installed in the chamber and baked, a rather large pressure rise was observed. After several bursts the pressure rise decreased, until there was none observable with a burst. These first few bursts are thought to clean the gas monolayer from the foil, a process equivalent to baking a vacuum system to outgas it. Moreover, on bursts where the pressure rise was observed, the electron output pulse was higher than when there was no observable pressure rise. If the electron output pulse from the oscilloscope photograph is graphically integrated to get the $\int_0^\infty V dt$ and this is divided by the resistance of the circuit and multiplied by the number of electrons per coulomb, one obtains the number of electrons released in a given laser burst. If the increase in the number of electrons released per laser burst when a pressure rise is observed is plotted against the observed

pressure rise, one obtains the curves of Fig. 5. (Most of the data for this experiment is plotted versus capacitor voltage to the laser flash light, Vc. For the relationship between laser input voltage and output power and energy, see Fig. 6) The relationship between the additional number of electrons ΔN_- observed accompanying a burst when a pressure rise is observed and the number of electrons observed for zero pressure rise is plotted in Fig. 7 for two metals, Al and Cu.

When the pressure rise no longer accompanied a laser burst, it was concluded that the gas monolayer had been cleared from the surface and that any electrons or positive ions that were collected were from the metals themselves and not from gases lodged on the surface of the metal. Data was taken by making a laser burst on the foil every 100 seconds, varying the input voltage to the laser with each successive burst. This was done for both polarities on the collector so that electrons as well as positive ions could be collected for each foil as a function of laser voltage with zero pressure rise. Taking the results from these runs, the maximum amplitude of the current from the foil could be calculated; from this value, when divided by the area of the laser spot, the maximum current densities from each metal could be calculated as a function of laser input voltage.

Graphs of current density vs flash lamp capacitor bank voltage are shown in Figs. 8 and 9 for $\approx 10^{-8}$ mm Hg base pressure and $\approx 5 \times 10^{-6}$ mm Hg base pressure, respectively. The decreased electron current density at higher pressure (10^{-6} mm) might be interpreted as electron loss mechanisms in the chamber. Two possibilities are:

1. Dissociative recombination,

$$O_2^+ + e^- \rightarrow 2O + \text{energy}$$

The recombination coefficient in this process is of the order of 10^{-6} and is energy dependent.

2. Dissociative attachment of electrons to O_2 molecules according to the equation

$$O_2 + e + 3 \text{ eV} \rightarrow O^- + O + \text{energy}$$

A quantitative calculation for this process cannot be done because the concentration that is time and position dependent is not known.

If the electron or positive ion output pulse shape is integrated, the total number of electrons or positive ions emitted by the foils can be obtained as a function of flash tube capacitor bank voltage. The resulting graphs of numbers of electrons and positive ions emitted as a function of the capacitor voltage are shown in Figs. 10, 11, 12, and 13. The numbers of particles in Figs. 10 and 12 were obtained at $\approx 10^{-8}$ mm Hg, and those of Figs. 11 and 13 are for $\approx 5 \times 10^{-6}$ mm Hg.

It is valuable to investigate the ratio of the number of electrons emitted at a base pressure of 10^{-6} mm Hg to the number of electrons emitted at 10^{-8} mm Hg. As can be seen from Fig. 14, the ratio is never as high as one except in the case of aluminum. This finding further supports the conclusion that one is actually measuring electrons from the foil rather than from the gas monolayer. If the measured output were coming from the gas on the surface, then when the vacuum was degraded to 5×10^{-6} mm Hg, the output would be expected to be higher than that obtained at high vacuum. The metals that were investigated all had a ratio very near to one except the stainless steel, which was approximately 1000 times lower for low vacuum than for high vacuum.

The ratio N_+/N_- at high vacuum was also analyzed and is plotted in Fig. 15. It was found that in the case of Be and Cu the ratio N_+/N_- is approximately 0.01, while that of aluminum is approximately 0.2.

Using the ratio of the number of positive ions to the number of electrons at 10^{-8} mm Hg and the Richardson-Smith equation[12] (Smith 1930), one can calculate the effective positive ion work functions for several of the metals. This was done by computing the ratio A_+/A_- of the constants in the Richardson equation

$$j_- = A_- T^2 e^{\frac{-\Phi_- e}{kT}}$$

and the Richardson-Smith equation

$$j_+ = A_+ T^2 e^{\frac{-\Phi_+ e}{kT}}$$

to obtain

$$\frac{j_+}{j_-} = \frac{M}{2M_e} e^{-\frac{(\Phi_+ - \Phi_-)e}{kT}}$$

Then, using the experimentally determined value of j_+/j_- to determine Φ_+ when Φ_- is known, the results of these calculations yield for Al, Be, and Cu the effective positive ion work functions of 5.3, 5.1, and 7.25 electron volts, respectively.

It was possible to obtain the experimental curves for electron current density vs input laser beam power and the positive ion current density vs input power. These are shown in Figs. 16 and 17.

From these curves one can determine the actual equations of charged particle current density vs input power. These equations are tabulated in Table II; it is seen that they are exponential in form, and further, that all the metals except gold have the same exponent for the electron current densities. In the case of very high input power, these simple exponential equations have to be modified by taking into account the space change limitations in the outcoming changed particle beams.

TABLE I

Metal	Surface temperature computed from Richardson equation
Al	1630°K
Ag	1900°K
Au	1940°K
Be	1430°K
Cu	1890°K
Stainless Steel	1830°K

TABLE II

Metal	Electrons	Ions
Al	$j = 5.2 \times 10^{-7}\ e^{3.5}\ P(kW)$	$j = 7.4 \times 10^{-8}\ e^{3.17}\ P(kW)$
Ag	$j = 2.05 \times 10^{-7}\ e^{3.5}\ P(kW)$	
S.S.	$j = 1.16 \times 10^{-7}\ e^{3.5}\ P(kW)$	
Cu	$j = 0.54 \times 10^{-7}\ e^{3.5}\ P(kW)$	$j = 0.733 \times 10^{-8}\ e^{2.42}\ P(kW)$
Be	$j = 0.14 \times 10^{-7}\ e^{3.5}\ P(kW)$	
Au	$j = 2.6 \times 10^{-12}\ e^{8.4}\ P(kW)$	

APPENDIX A

Physical Constants Used in This Experiment

Metal	K $\left(\frac{\text{Cal}}{\text{cm sec }^{\circ}\text{C}}\right)$	C $\left(\frac{\text{Cal}}{\text{gm }^{\circ}\text{C}}\right)$	ρ $\left(\frac{\text{gm}}{\text{cm}^3}\right)$	κ $\left(\frac{\text{cm}^2}{\text{sec}}\right)$	Φ (electron volts)	$\Phi e/k$ ($^{\circ}$K)
Al	1.01	0.277	2.7	1.35	3.6	4.178×10^4
Ag	0.992	0.076	10.5	1.24	4.4	5.106×10^4
Au	0.703	0.0314	19.3	1.16	4.6	5.338×10^4
Be	0.35	0.505	1.85	0.37	3.5	4.062×10^4
Cu	0.858	0.093	8.92	1.03	4.6	5.338×10^4
S.S.	0.107	0.157	7.75	0.088	4.3	4.990×10^4

K thermal conductivity

C heat capacity

ρ density

κ thermal diffusivity = $\frac{K}{\rho C}$

Φ work function (electron volts)

$\frac{\Phi e}{k}$ work function ($^{\circ}$K)

k Boltzmann constant

APPENDIX B

The Spreading Gaussian Approximation

Assume the beam spot has a gaussian temperature distribution and that at any point in time the average temperature of the spot is represented by one-half of the maximum height of the gaussian and the width of the spot is the full width at one-half maximum. Then in two dimensions

$$< r^2 > = 4\kappa t \tag{1}$$

where t is the time, κ is the thermal diffusivity, and r is the distance from the gaussian center. The temperature $T(r,t)$ will be given by

$$T(r,t) = \frac{T_o}{8\pi\kappa t} e^{-\frac{r^2}{8\kappa t}} \tag{2}$$

where T_o is a constant.

The full width at one-half maximum is given by

$$d = 2.36 < r > = 4.72 \sqrt{kt}$$

and the actual beam spot diameter $d = 1.42$ mm.

Then, using Eq. (2), one can consider the time and space development of the diffusion in the case where the incident spot radius is r_o, as shown below, and at successive times the spot size grows as the foil heats up but the temperature decreases over the spot. Consider the following notation:

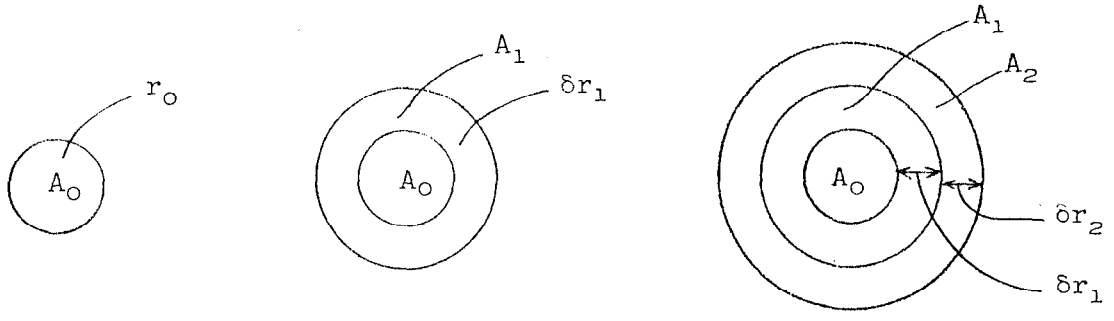

time $t = t_o$ $t = t_1$ $t = t_2$

$A_o = \pi r_o^2$	at Temperature	T_{oo}	at	time	t_o
$A_o = \pi r_o^2$	at Temperature	T_{1o}	at	time	t_1
$A_o = \pi r_o^2$	at Temperature	T_{2o}	at	time	t_2
$A_1 = 2\pi r_o \delta r$	at Temperature	T_{11}	at	time	t_1
$A_1 = 2\pi r_o \delta r$	at Temperature	T_{21}	at	time	t_2
$A_2 = 2\pi(r_o + \delta r)\delta r$	at Temperature	T_{12}	at	time	t_2

Thus the temperature of the growing beam spot segment with an area A_n at time t_ℓ and radius from center r_m will be given as $T_n(t_\ell, r_m)$ by the expression

$$T_{ij} = T(t_\ell, r_m) = \frac{T_o}{8\pi\kappa(t_o + \ell\delta t)} e^{-\frac{(r_o + m\delta r_m)^2}{8\kappa(t_o + \ell\delta t)}} \qquad (3)$$

where δt can be arbitrarily chosen as a suitably small increment of time, and $r_o = \frac{d}{2}$ is the initial spot radius. Using Eq. (1), δr_m is then calculated as the radius that the beam spot will spread in a time increment δt:

$$\delta r_m = \frac{4k\delta t}{2r_{m-1}} = \frac{2k\delta t}{r_{m-1}}$$

Using the actual spot size as found in the experiment, t_o can now be calculated. In this case t_o is interpreted to be the time that it would take a point source of temperature to grow to the beam spot size. Using $r_o = 0.71$ mm yields a value for t_o of $\frac{9.05 \times 10^{-4}}{\kappa}$ sec.

From Eq. (3), using the previously calculated peak surface temperatures from the Richardson equation and the values found for r_o, t_o, δr and δt, t_o can be calculated. Then at any time t_i the total current emitted is given by

$$i(t_i) = \sum_j j(T_{ij})A_j$$

where T_{ij} is defined by Eq. (3). The result of this calculation is shown in Fig. 4.

LIST OF REFERENCES

1. W.I. Linlor, Appl. Phys. Letters 3, 210 (1963).
2. W.I. Linlor, Bull. Am. Phys. Soc. 7, 440 (1962).
3. J.J. Muray, Bull. Am. Phys. Soc. 8, 77 (1963).
4. J.J. Muray, Dielectrics 221 (February 1964).
5. R.E. Honig and J.R. Woolston, Appl. Phys. Letters 2, 138 (1963).
6. D. Lichtman and J.F. Ready, Phys. Rev. Letters 10, 342 (1963).
7. C.M. Verber and A.H. Adelman, Appl. Phys. Letters 2, 220 (1963).
8. R.E. Honig, Appl. Phys. Letters 3, 8 (1963).
9. J.F. Ready, Appl. Phys. Letters 3, 11 (1963).
10. F. Giori, L.A. MacKenzie, and E.J. McKinney, Appl. Phys. Letters 3, 25 (1963).
11. D. Lichtman and J.F. Ready, Appl. Phys. Letters 3, 115 (1963).
12. L.P. Smith, Phys. Rev. 35, 381 (1930).

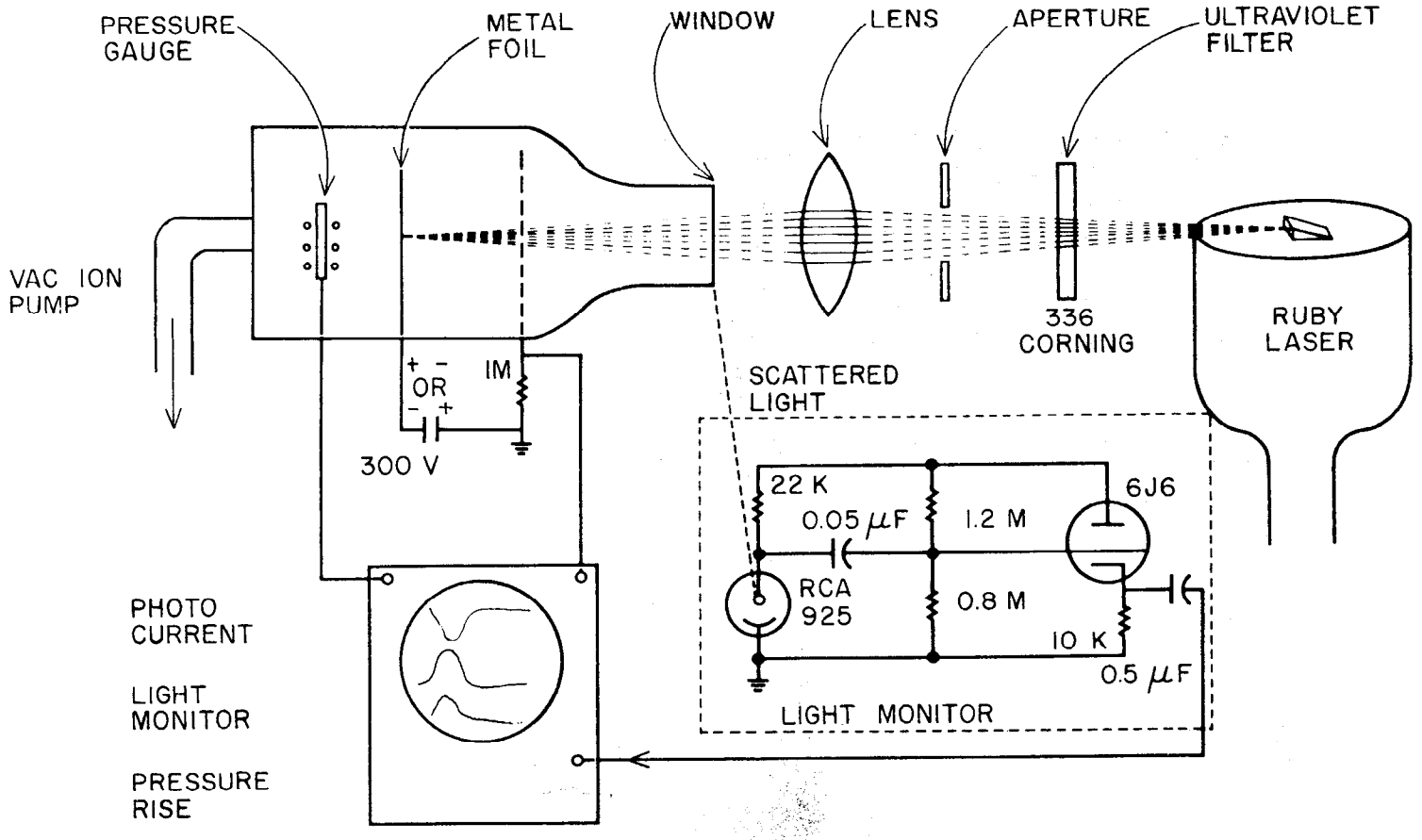

FIG. 1--THE SCHEMATIC DIAGRAM OF THE EXPERIMENTAL ARRANGEMENT. 84-10-A

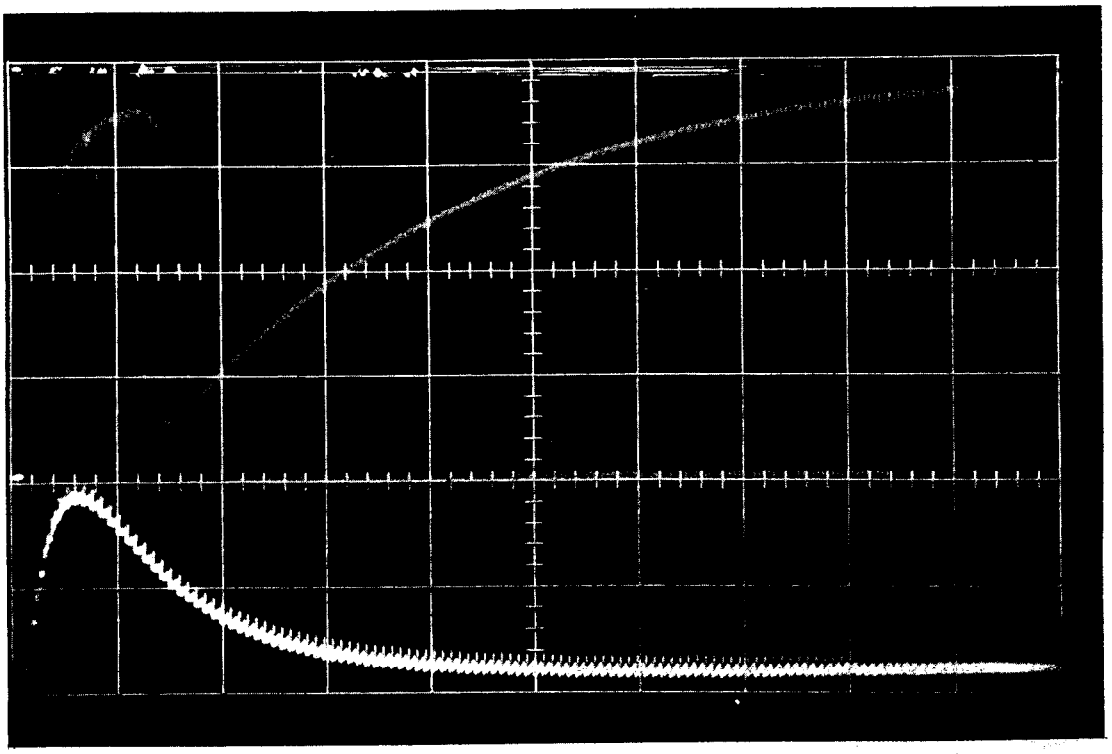

FIG. 2--Typical oscilloscope photograph

This picture shows on top trace the collected electron current waveform as a function of the time (horizontal speed 50 μsec/cm); on the second trace the light intensity of the laser beam as function of the time is shown (50 μsec/cm), and on the bottom trace the pressure rise is depicted vs time. (Here the horizontal speed is 200 msec/cm.)

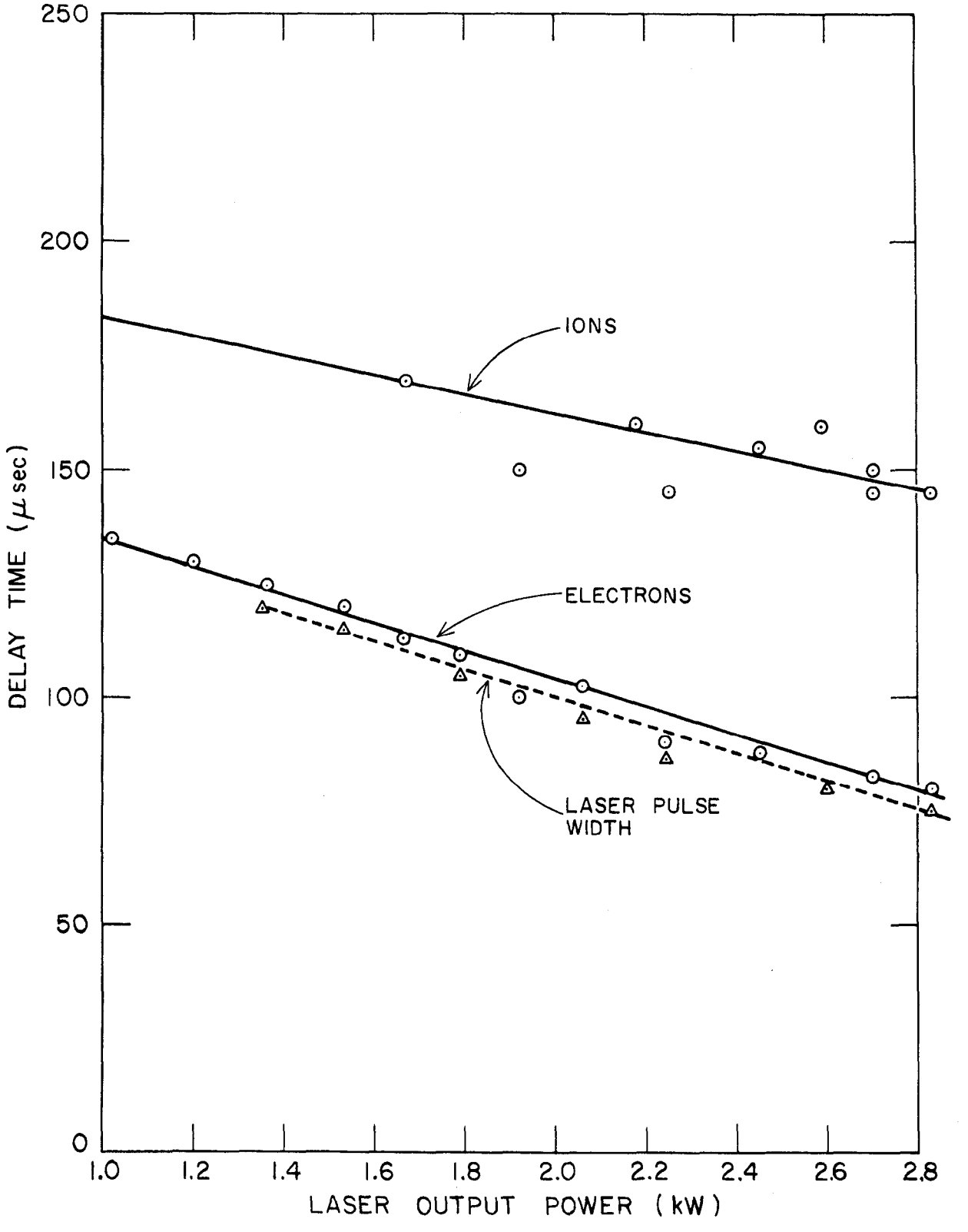

FIG. 3 -- DELAY TIME OF THE PEAK ELECTRON AND ION PULSE vs LASER OUTPUT POWER.

84-12-A

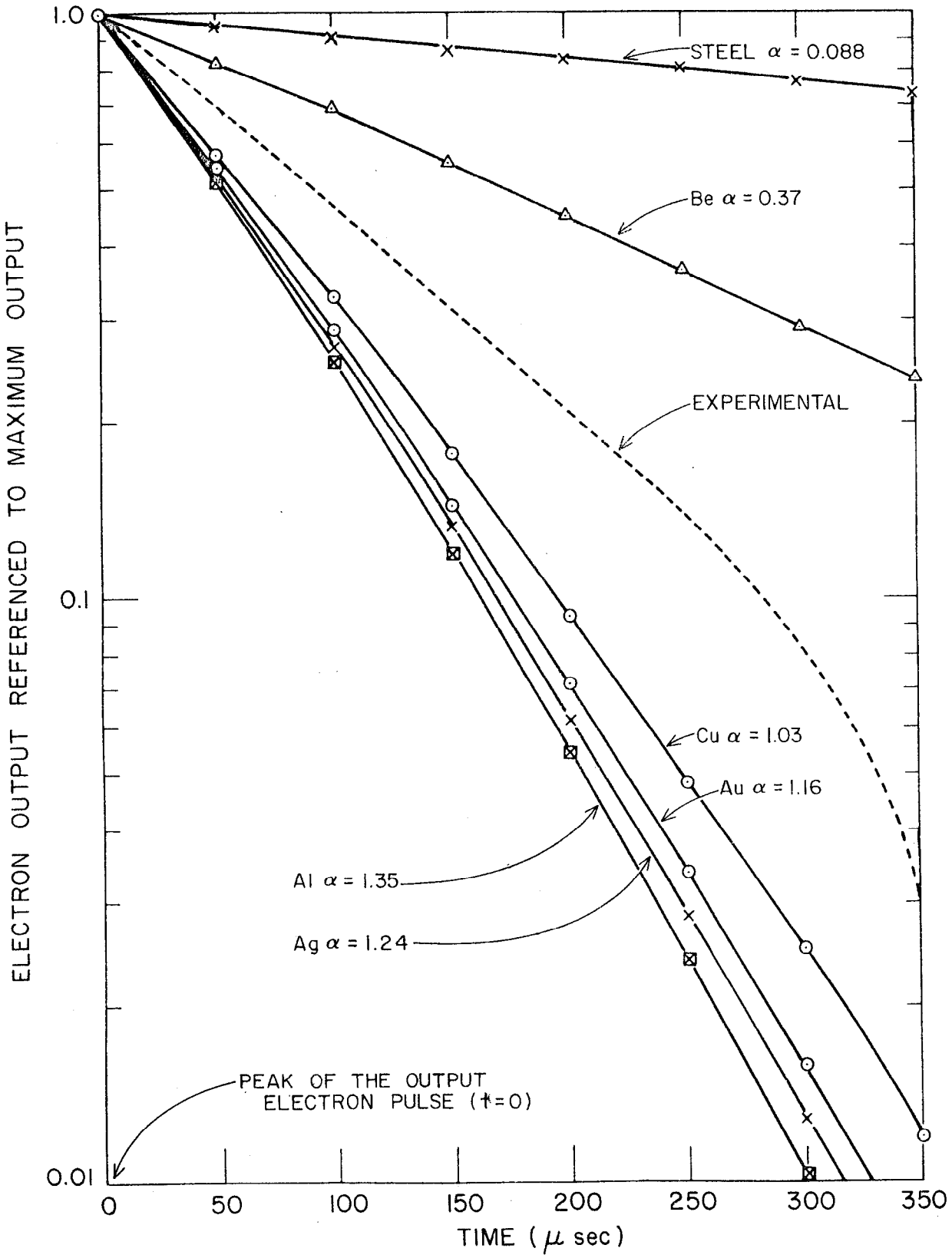

FIG. 4--OUTPUT DECAY COMPUTED FROM HEAT CONDUCTION EQUATION ASSUMING DECAYING GAUSSIAN.

84-8-A

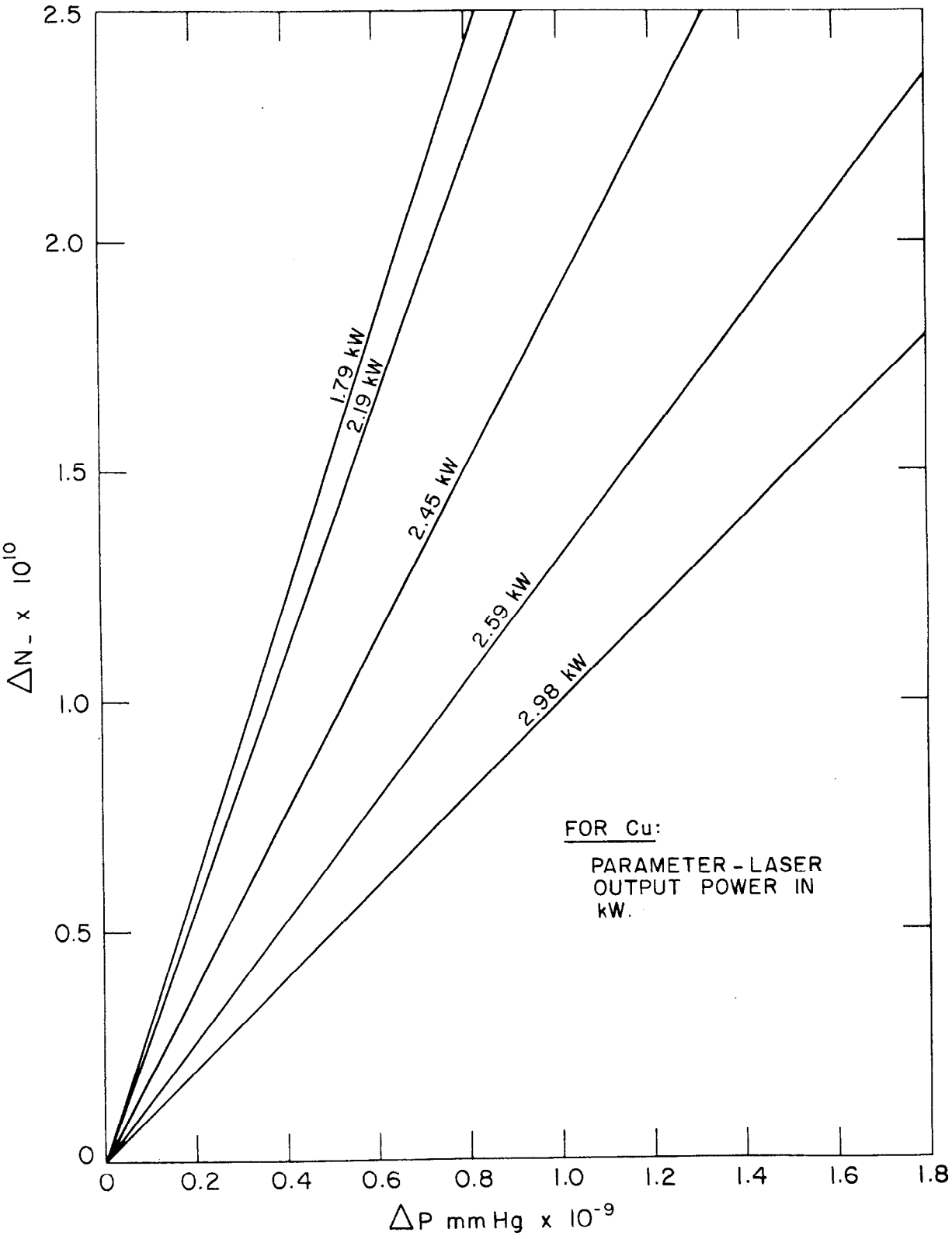

FIG. 5--ELECTRON OUTPUT vs PRESSURE RISE.

84-7-A

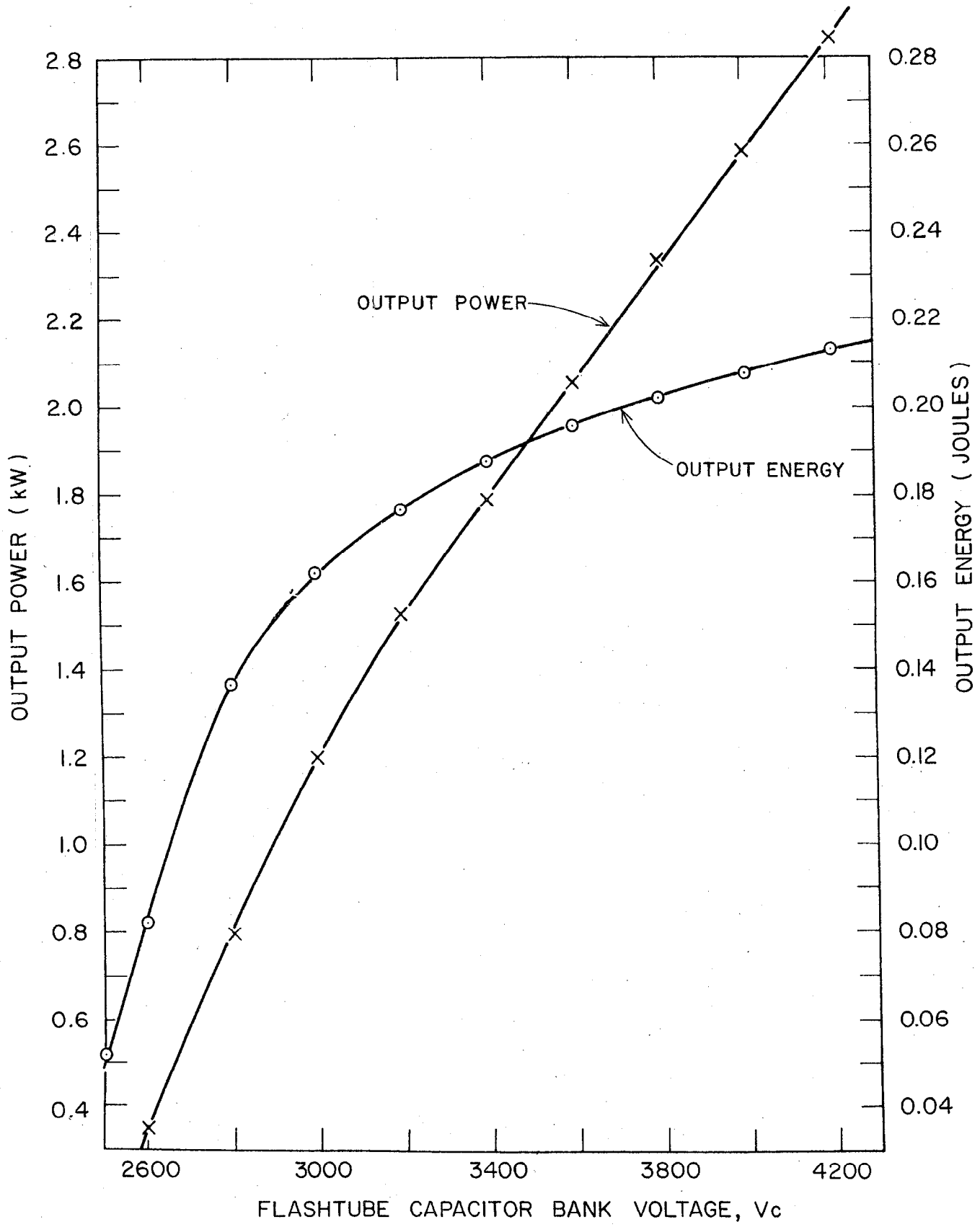
OUTPUT POWER
OUTPUT ENERGY
OUTPUT POWER (kW)
OUTPUT ENERGY (JOULES)
FLASHTUBE CAPACITOR BANK VOLTAGE, Vc
2.8
2.6
2.4
2.2
2.0
1.8
1.6
1.4
1.2
1.0
0.8
0.6
0.4
0.28
0.26
0.24
0.22
0.20
0.18
0.16
0.14
0.12
0.10
0.08
0.06
0.04
2600
3000
3400
3800
4200

FIG. 6

84-4-A

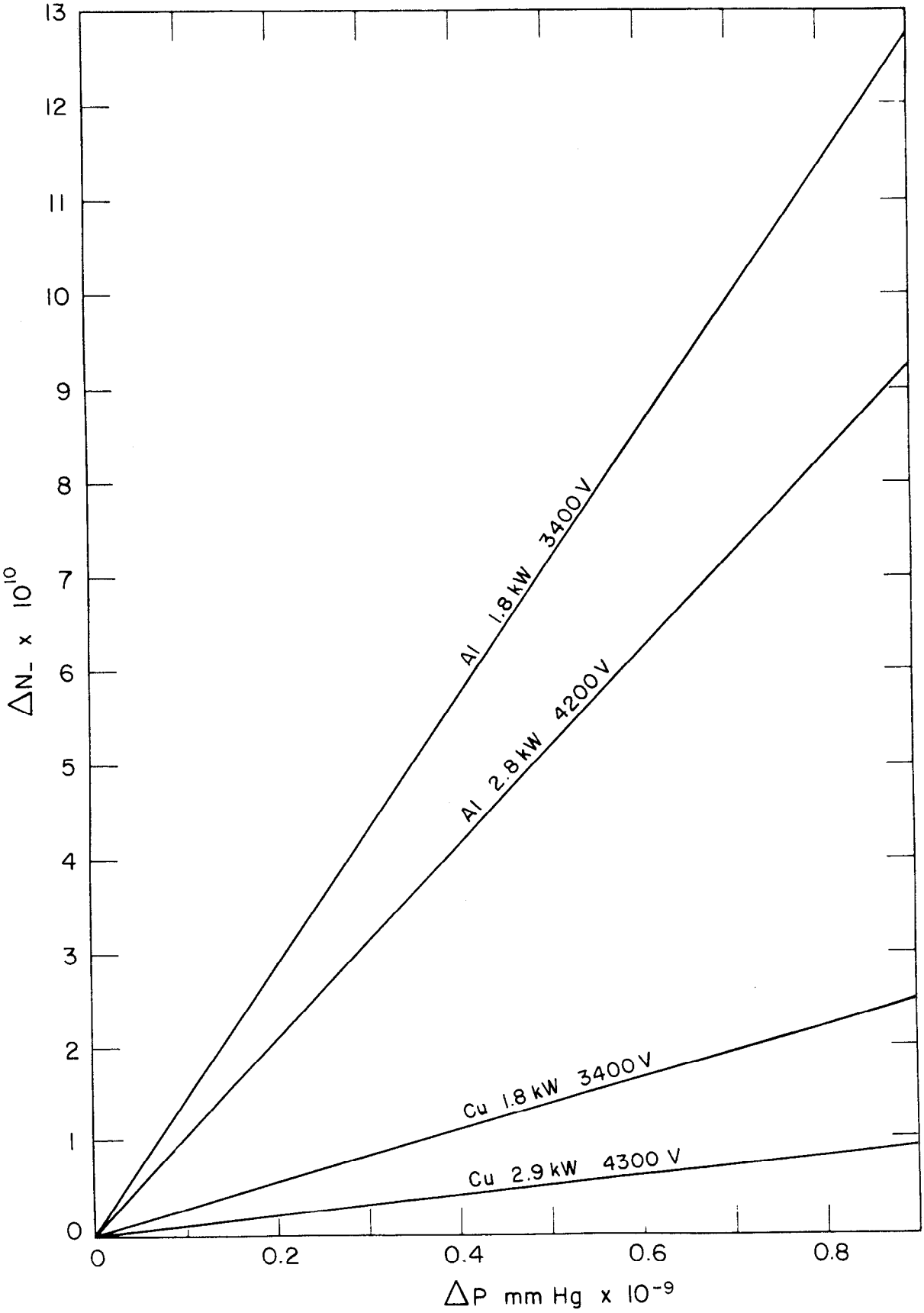

FIG. 7 -- ΔN_- vs PRESSURE RISE.

84-14-A

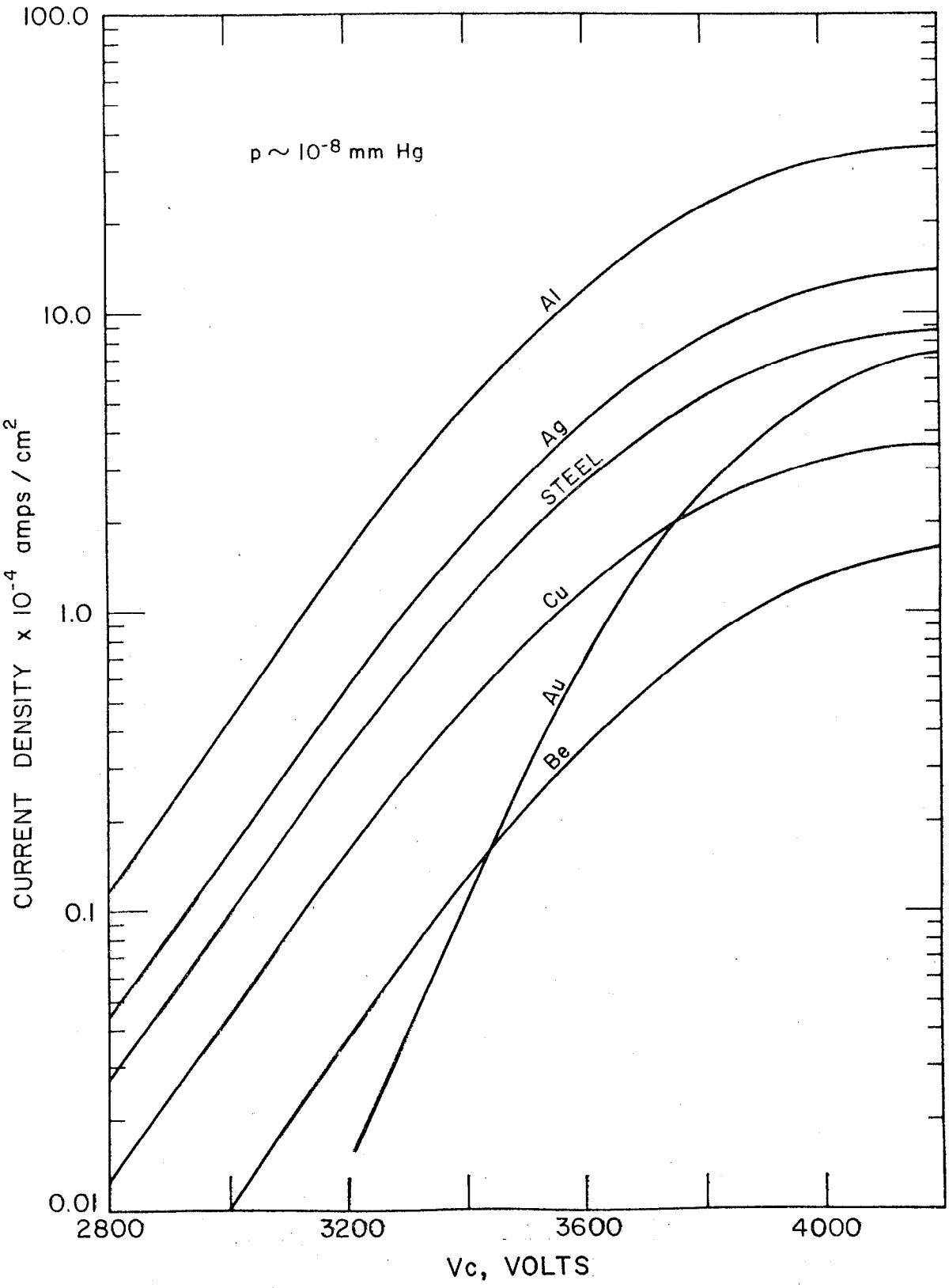

FIG. 8--ELECTRON CURRENT DENSITY vs CAPACITOR BANK VOLTAGE.

84-6-A

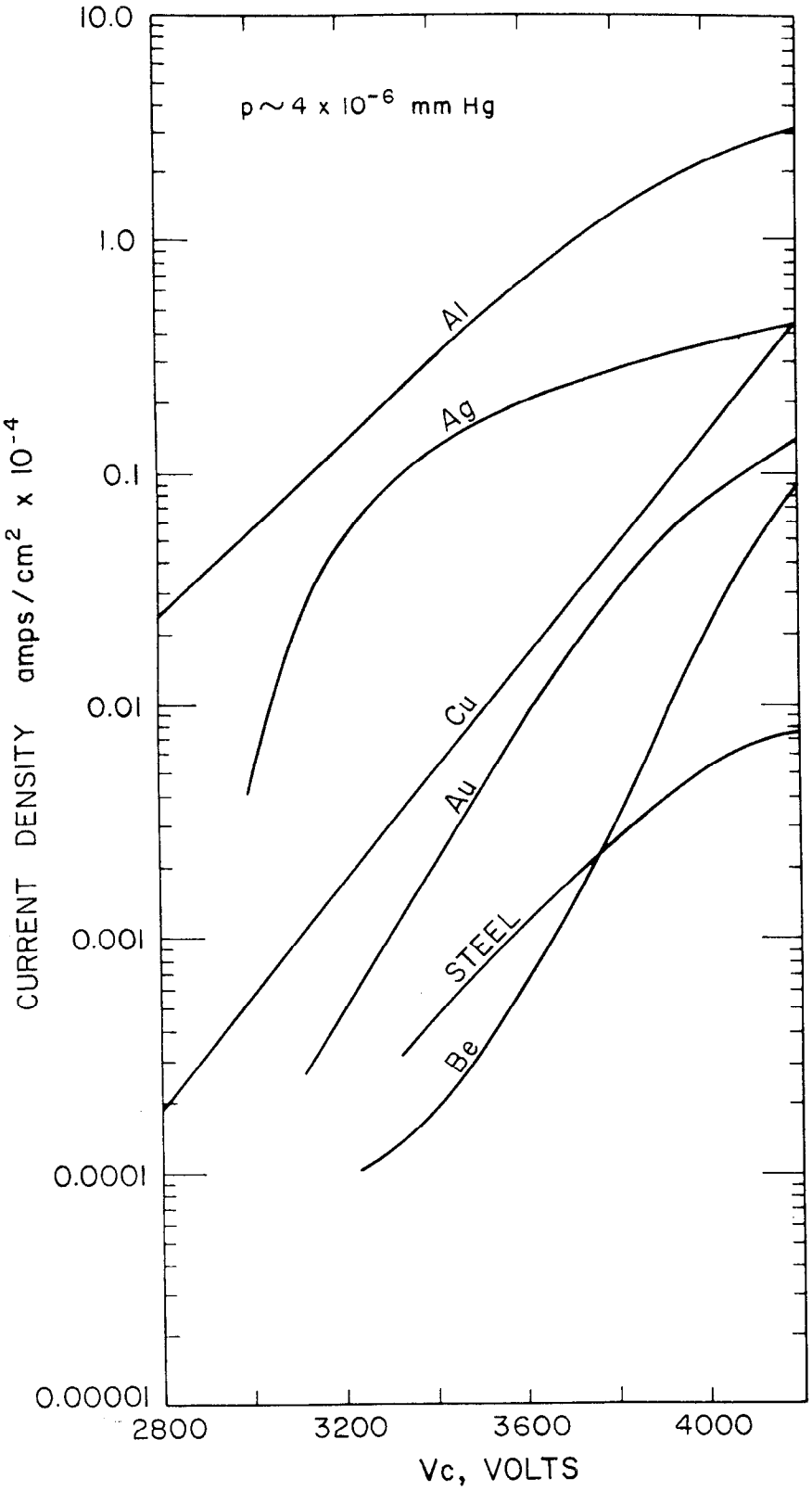

FIG. 9 -- ELECTRON CURRENT DENSITY vs VOLTAGE.

84-2-A

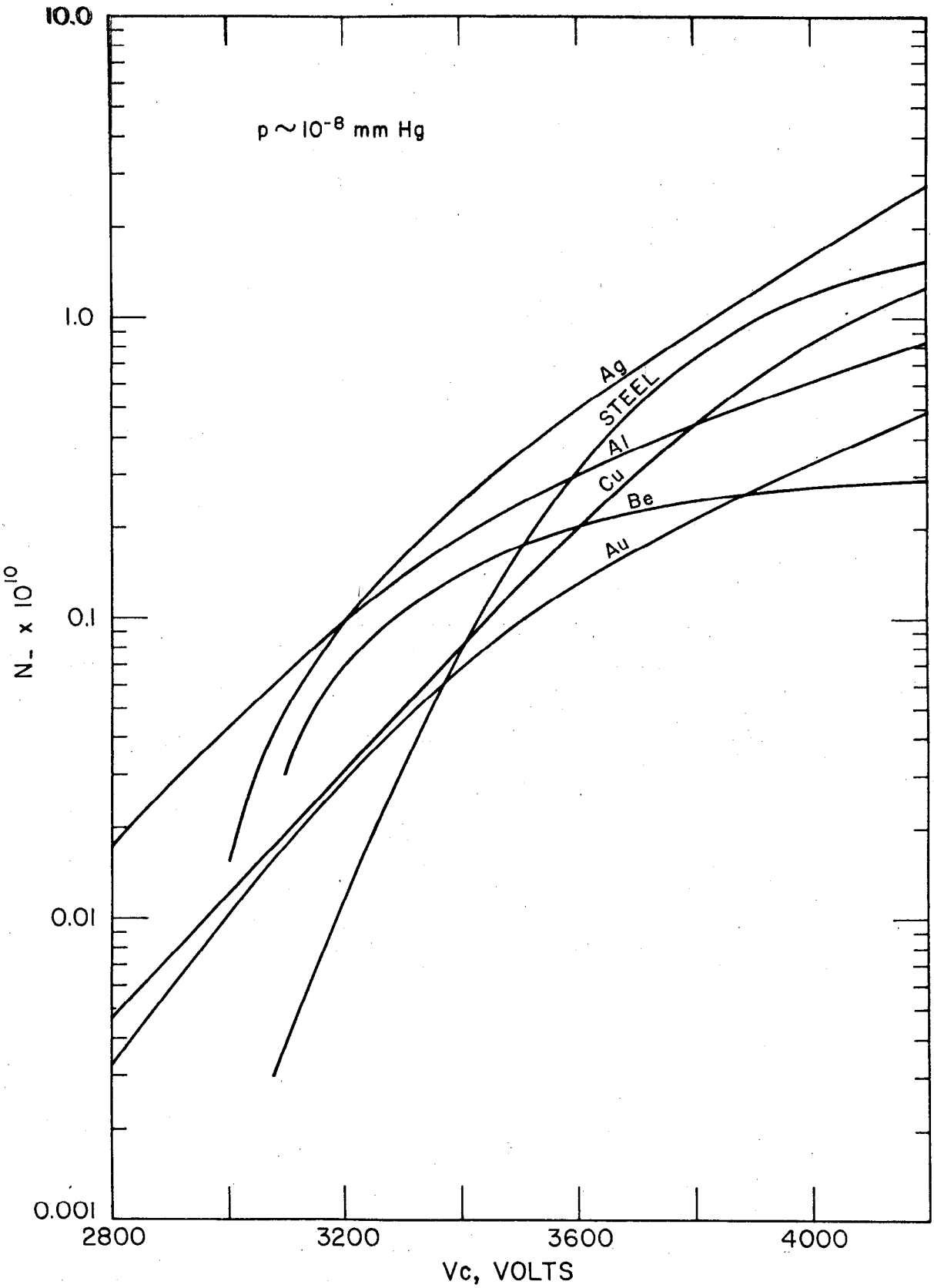

FIG. 10--ELECTRON OUTPUT vs VOLTAGE.

84-5-A

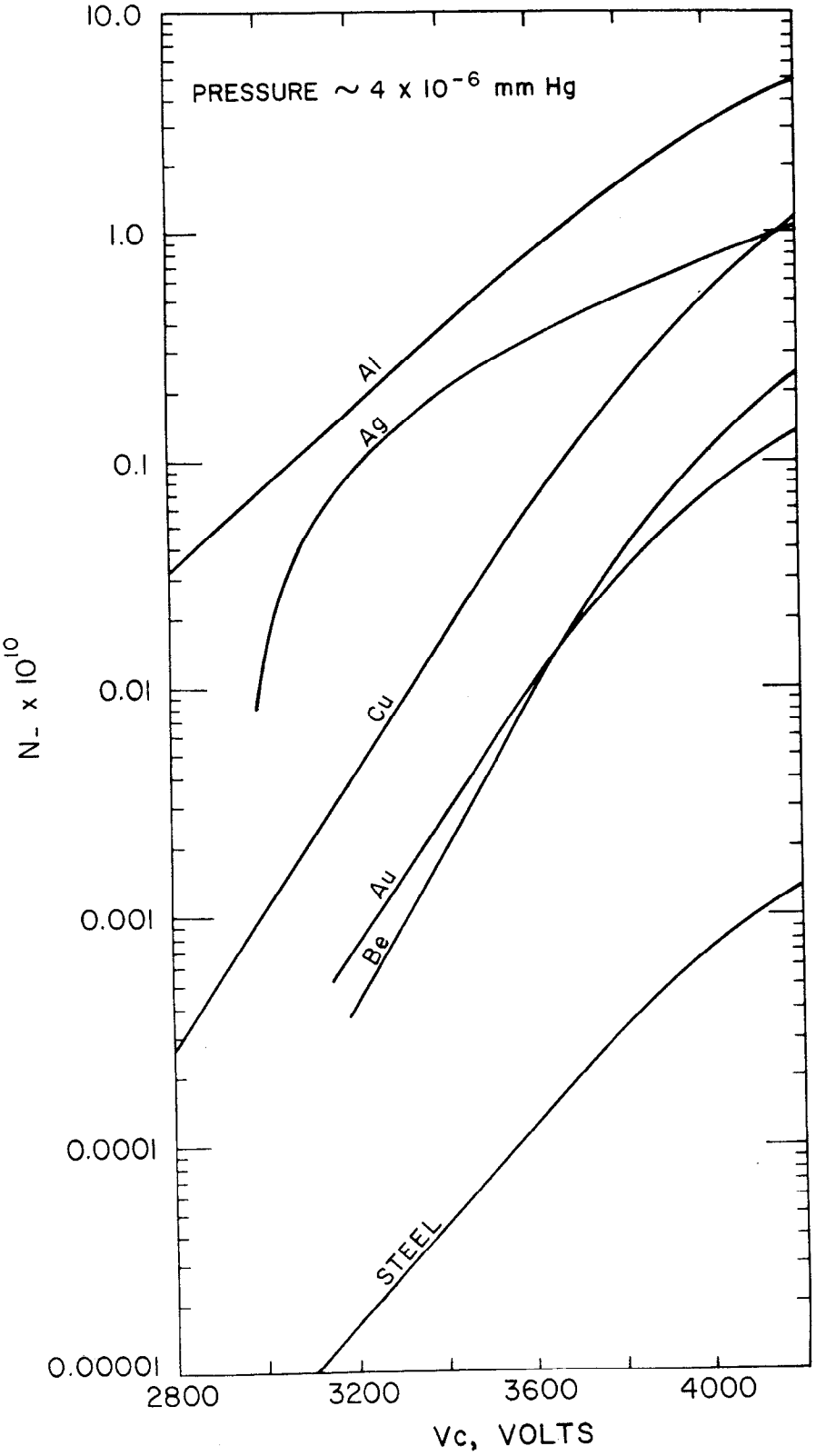

FIG. 11--ELECTRON OUTPUT FROM FOILS.

84-1-A

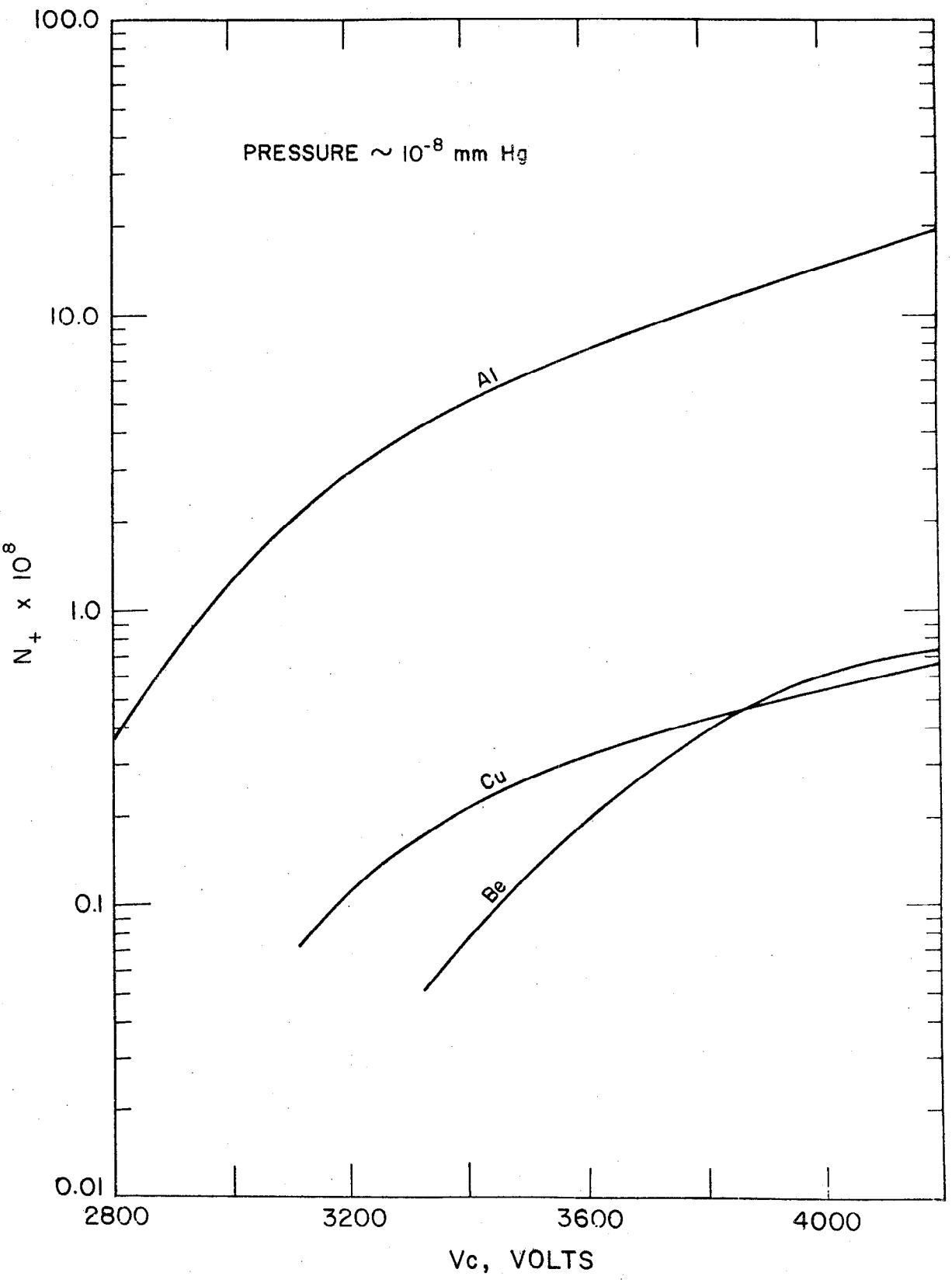

FIG. 12--NUMBER OF COLLECTED IONS vs VOLTAGE. 84-16-A

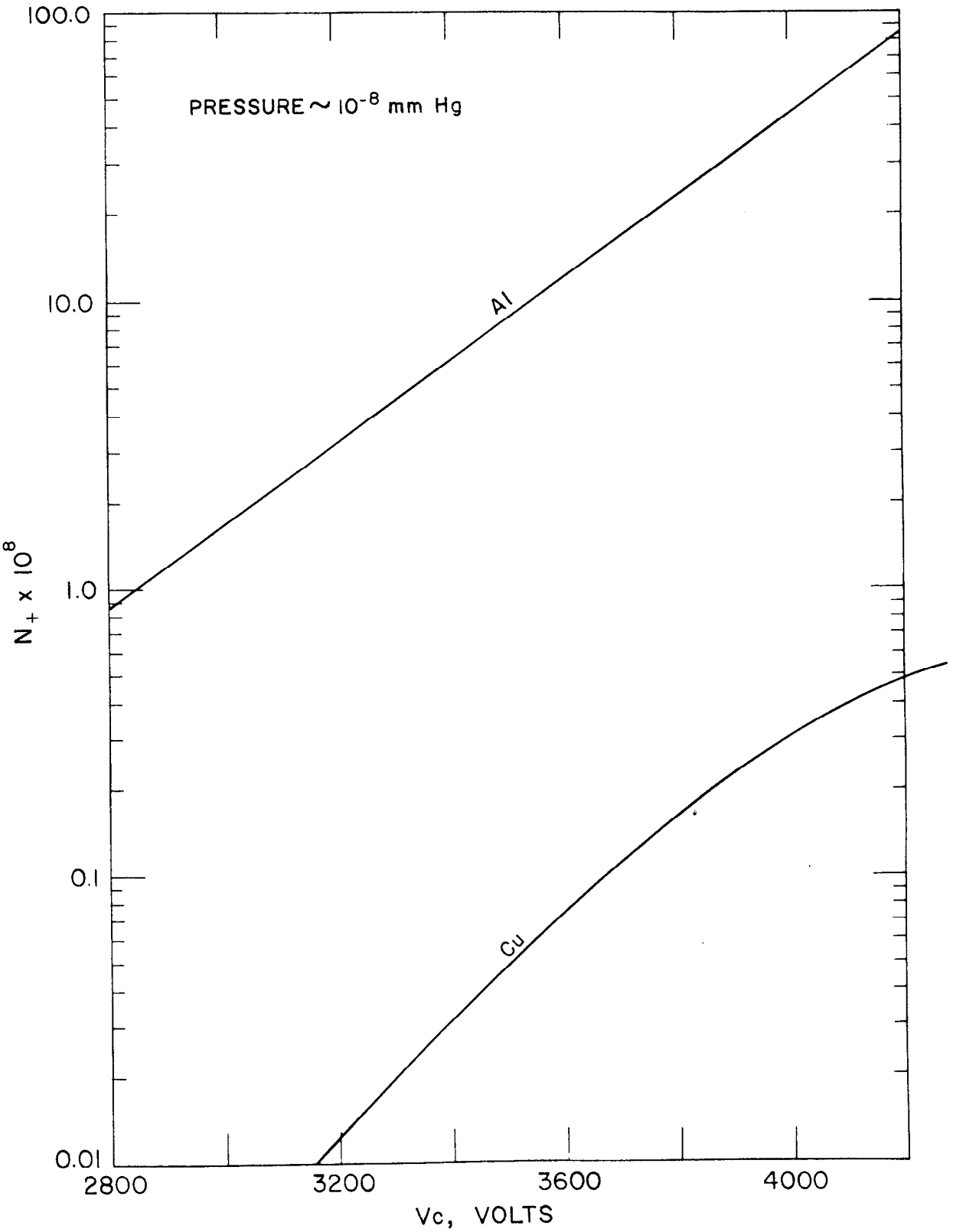

FIG. 13 -- NUMBER OF IONS COLLECTED vs VOLTAGE. 84-9-A

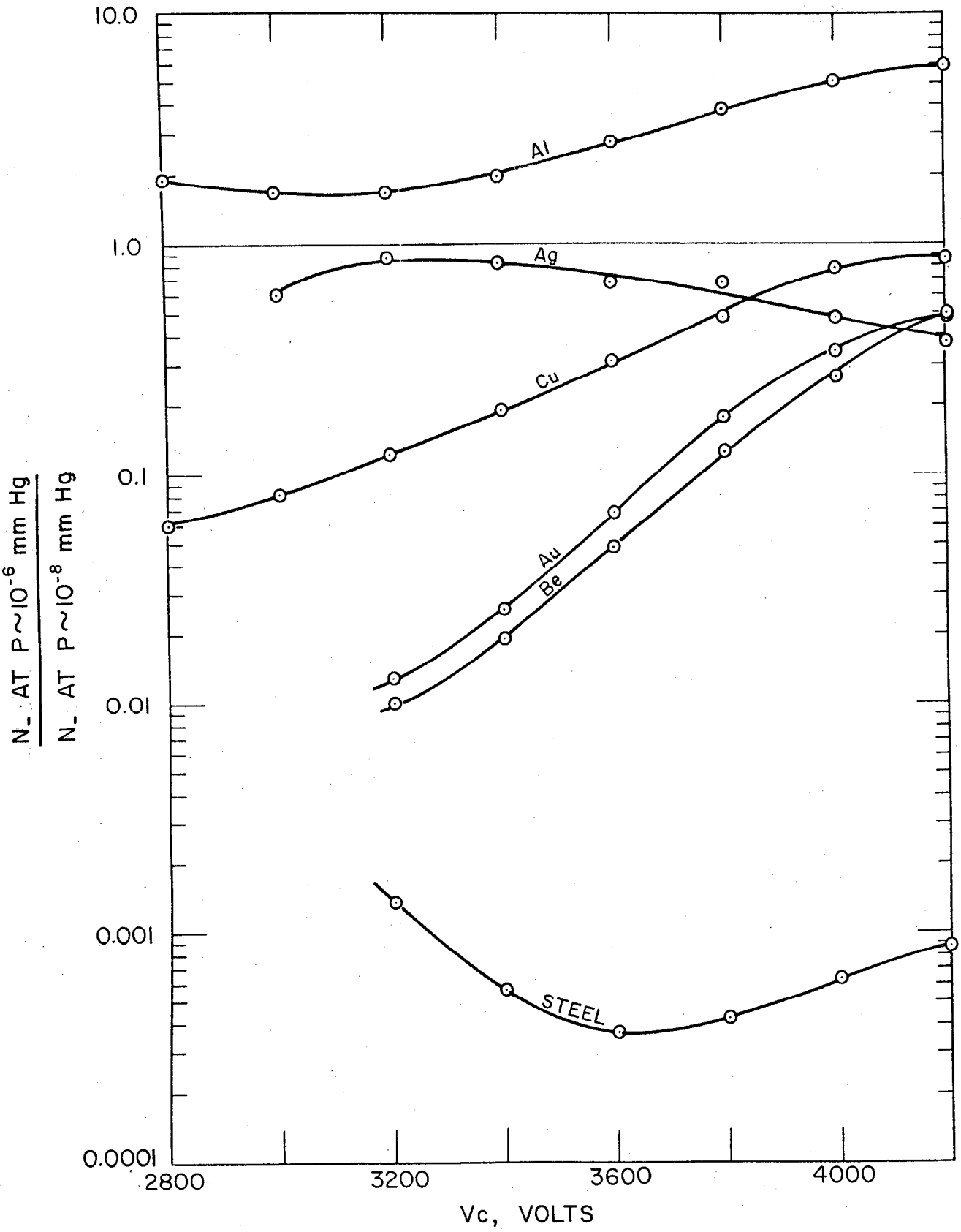

FIG. 14--THE RATIO OF ELECTRON OUTPUTS AT DIFFERENT PRESSURES vs VOLTAGE.

84-3-A

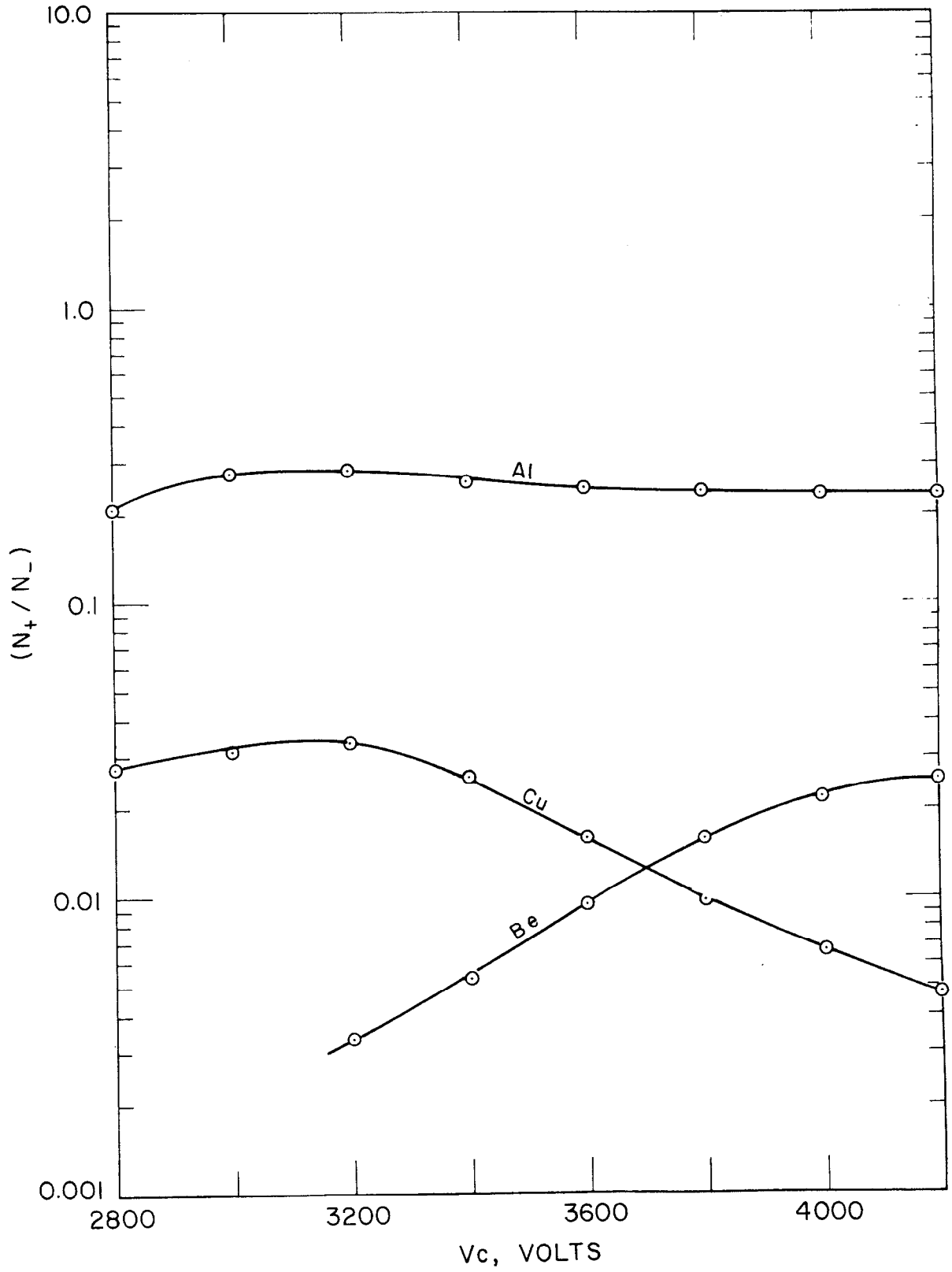

FIG. 15--RATIO (N_+ / N_-) FOR $\Delta P \sim 0$ AT $\sim 10^{-8}$ mm Hg vs VOLTAGE.

84-13-A

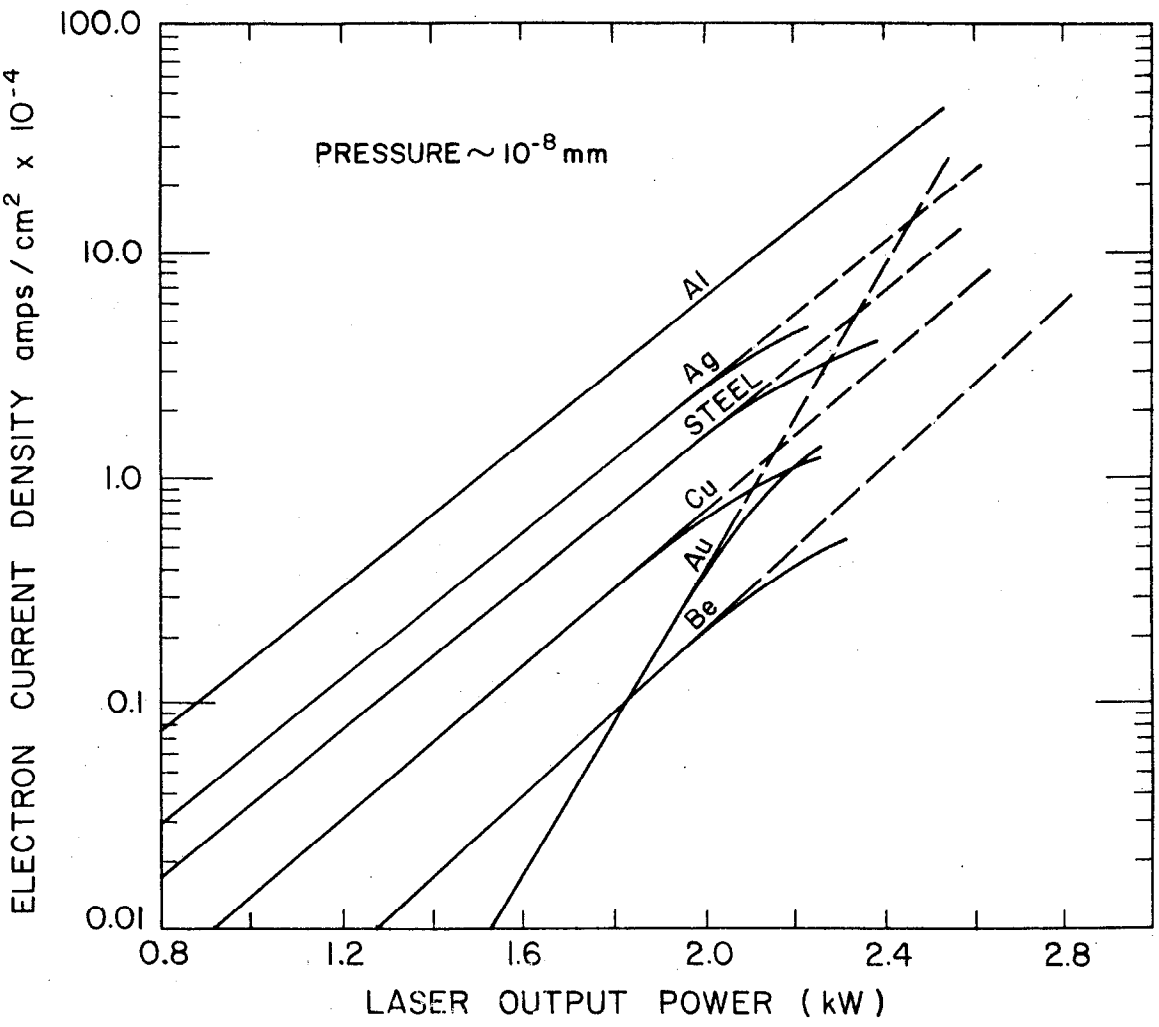

FIG. 16--ELECTRON CURRENT DENSITY vs POWER. 84-11-A

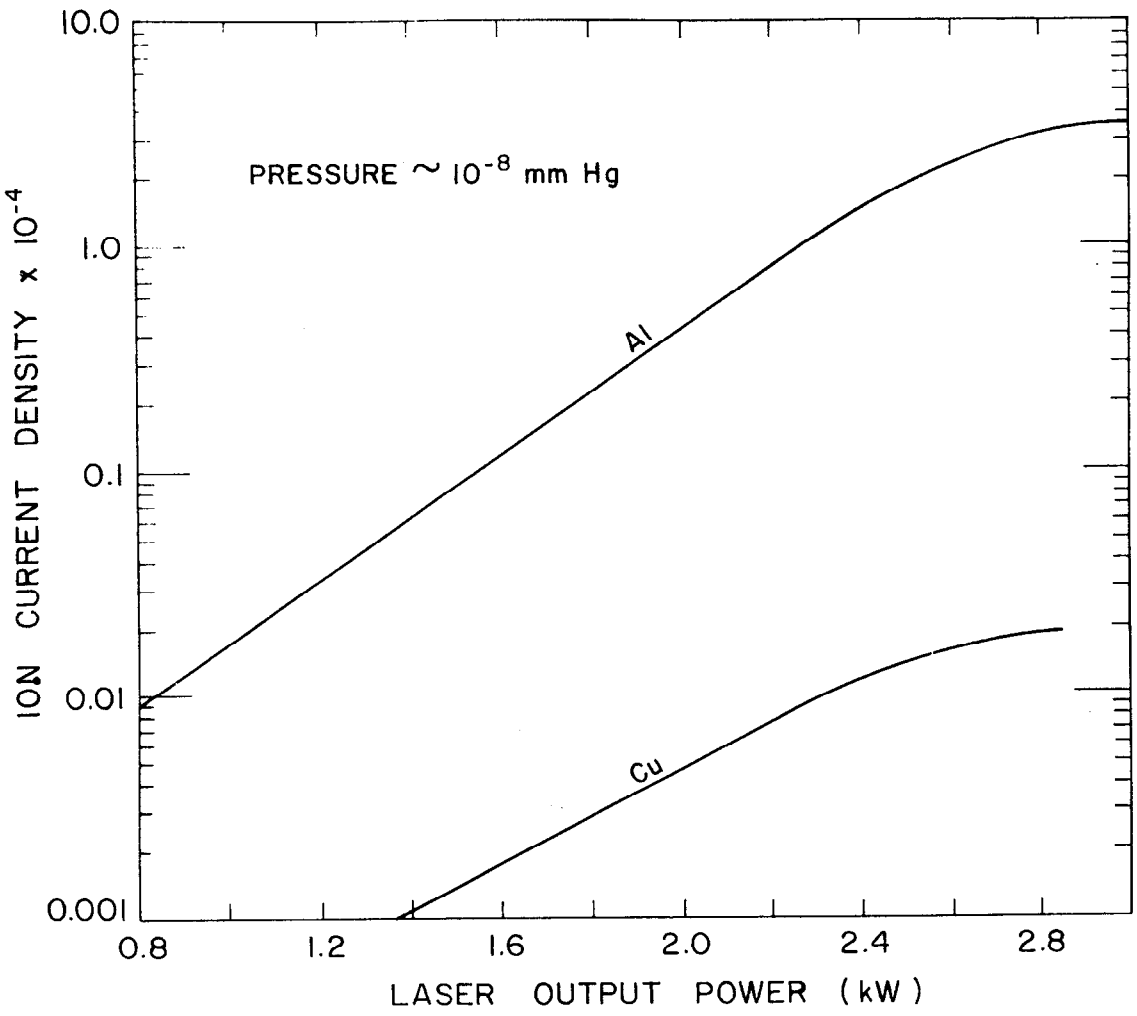

FIG. 17--POSITIVE ION CURRENT DENSITY vs POWER.

84-15-A